Biomimetic morphological design for manganese oxide and cobalt hydroxide nanoflakes with a mosaic interior†‡

Yuya Oaki and Hiroaki Imai*

Received 29th September 2006, Accepted 16th November 2006
First published as an Advance Article on the web 11th December 2006
DOI: 10.1039/b614191a

We synthesized manganese oxide and cobalt hydroxide nanoflakes with mosaic interiors in aqueous solutions containing poly(acrylic acid) and poly(ethyleneimine), respectively. Nanocrystals 2–3 nm in size made up the mosaic interiors and oriented architectures in the flakes less than 100 nm in width and 10 nm in thickness. The organic polymers coordinated to the metal ionic species and interacted with the growing crystals. These two interaction styles of the polymers led to morphological evolution at a nanoscopic scale. The results indicate that tailoring an interaction between organic and inorganic molecules realizes a practical application of a biomimetic approach to the design and integration of functional nanomaterials.

1. Introduction

Nanomaterials hold significant potential for novel applications that are not conceivable with present technologies. The fabrication of low-dimensional nanomaterials, including particles, rods, wires, belts, tubes, and sheets, has been well demonstrated in recent studies. Two-dimensional (2D) nanomaterials have especially attracted interest in the past decade because of their great potential for generating versatile structures and properties.[1–17] On the other hand, the integration of modular nanomaterials is an important challenge in the next stage of materials science.[17–19] Tailoring the hierarchical organization can lead to emergent properties beyond the mere aggregation of building blocks.

Biominerals have inspired novel approaches for the generation of hierarchically structured materials under ambient conditions. Biomimetic crystal design using polymers has been well-demonstrated in various systems especially in terms of the morphology changes.[20] We have investigated nanocrystal engineering in biominerals and biomimetic materials.[21,22] An exquisite association of organic molecules plays multiple roles for crystal growth and morphogenesis, in terms of coordination to inorganic species and specific adsorption to the growing crystals. As well as the fundamental study of morphological evolution, widespread application to functional materials is a current challenge for the further development of biomimetic materials chemistry.

Manganese- and cobalt-related materials are of central importance for technological applications because of their electrochemical, magnetic, and catalytic properties.[23–36] The design of nanoscopic structures incorporating these metals promises to improve their properties further. Although various crystal structures and morphologies of manganese oxides were synthesized in earlier work, the reaction and treatment were carried out at high temperature in most cases. Room-temperature synthesis was achieved in the case of Mn_3O_4 nanocrystals.[30] The exfoliation of the layered structure led to the formation of nanosheets of birnessite-type manganese oxide, but the precursor layered compound was synthesized by solid sate reaction at a high temperature.[28] Plate and sheet-like morphologies of manganese oxide and cobalt hydroxide were fabricated by various synthetic routes, but the morphological control was performed at the submicrometric scale.[23,27,31–34] It is not so easy to generate hierarchical structures such as 2D nanomaterials consisting of 1D building blocks using the present methods. Biomimetic pathways would realize the hierarchical crystal design of functional metal oxides and hydroxides, as is the case with biomineralization.

In the present study, we generated manganese oxide and cobalt hydroxide nanoflakes with a mosaic interior through a biomimetic approach under ambient conditions. These mosaic nanoflakes were made by the oriented architectures of the nanocrystals with the incorporation of polymers: poly(acrylic acid) (PAA) and poly(ethyleneimine) (PEI) mediated the integration of manganese and cobalt hydroxide nanocrystals, respectively (Chart 1).

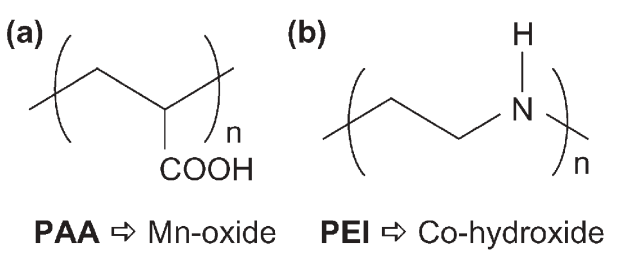

Chart 1 Structural formulae for PAA (a) and PEI (b).

Department of Applied Chemistry, Faculty of Science and Technology, Keio University, 3-14-1Hiyoshi, Kohoku-ku, Yokohama, 223-8522 Japan. E-mail: hiroaki@applc.keio.ac.jp; Fax: +81 45 566 1551; Tel: +81 45 566 1556

† Electronic supplementary information (ESI) available: Electron microscope images and XRD patterns of the materials synthesized without additives. See DOI: 10.1039/b614191a

‡ The HTML version of this article has been enhanced with colour images.

2. Experimental

2.1. Materials and procedure

The stock solutions containing 20 mM manganese chloride tetrahydrate ($MnCl_2{\cdot}4H_2O$, Kanto Chemical, 99.0%) and 20 mM PAA (Mw 2000, Aldrich Chemical) were prepared using purified water in polystyrene or glass bottles. In this report, the polymer concentration is represented by the contents of a monomeric unit. An equal volume of 200 mM sodium hydroxide (NaOH, Junsei Chemical, 96.0%) was separately prepared in a glass beaker and was then added to the stock solution without stirring at room temperature. The mixture was maintained at 25 °C in the closed sample bottle. The slightly turbid mixture was centrifuged within 12 hours of mixing. The supernatant liquid was dropped on a copper grid supported with a collodion membrane, a glass slide and a silicon substrate. For the synthesis of cobalt hydroxide, cobalt chloride hexahydrate ($CoCl_2{\cdot}6H_2O$, Kanto Chemical, 99.0%) and PEI (Mw 60000, 50 wt.-% aqueous solution, Acros Organics) were included in the precursor solution instead of $MnCl_2{\cdot}4H_2O$ and PAA (Chart 1). The other experimental conditions, including the concentration and procedure, were the same as those for manganese oxide. In the case of cobalt hydroxide, the flakes were collected by centrifugation for approximately 90 minutes and were dried at room temperature.

2.2. Characterization

The morphologies of the resultant materials were characterized by a field-emission scanning electron microscope (FESEM, FEI Sirion) operated at 2.0 kV and a field-emission transmission electron microscope (FETEM, FEI Tecnai F20) operated at 200 kV. FETEM analysis was performed by the following means: high-resolution observation (HRTEM) with its fast-Fourier transform image (FFT), high-angle-annular dark-field of scanning transmission detection (HAADF-STEM), energy-dispersive X-ray analysis (EDX, EDAX r-TEM 32), selected-area electron diffraction (SAED), and electron energy-loss spectroscopy (EELS, Gatan, Imaging Filter model 607). For manganese oxide, the incorporated PAA molecules were characterized by a reflection mode using Fourier transform infrared spectroscopy (FT-IR, Smiths Detection, illuminatIR II). As a reference, commerical PAA powders including sodium salt and acid salt were analyzed by a KBr method using another FT-IR (Bio-Rad, FTS 60A). For cobalt hydroxide, additional characterization was carried out by using powdered X-ray diffraction (XRD, Bruker AXS, D8 Advance with Cu-Kα radiation and graphite monochromator), FT-IR (Bio-Rad, FTS 60A), UV-Vis spectra recorded by spectrophotometer at room-temperature (JASCO, V-560), and elemental analysis of organic molecules (CHN analysis, Vario EL, Elementar).

3. Results

3.1. Synthesis and characterization of manganese oxide nanoflakes

A clear orange liquid was immediately obtained upon mixing the Mn^{2+}/PAA and NaOH solutions. The liquid became slightly turbid over several hours of mixing. After centrifugation of the turbid substance, Tyndall light scattering was observed in the transparent orange liquid (inset of Fig. 1a), suggesting that the nanomaterials were dispersed in the liquid. Hexagonal nanoflakes *ca.* 50 nm in size were observed in the FETEM and HAADF-STEM images (Fig. 1a,b). The magnified HAADF-STEM image revealed that the flake was made up of a mosaic structure of nanograins 2–3 nm in size (Fig. 1c). Through several FESEM images, the thickness of a nanoflake was estimated to be approximately 10 nm (Fig. 1d,e). The peaks of carbon, oxygen, and manganese were detected in the EDX spectrum. The enhanced carbon peak implies the formation of a manganese oxide–PAA composite material, even though the peaks of carbon, oxygen, and copper are also

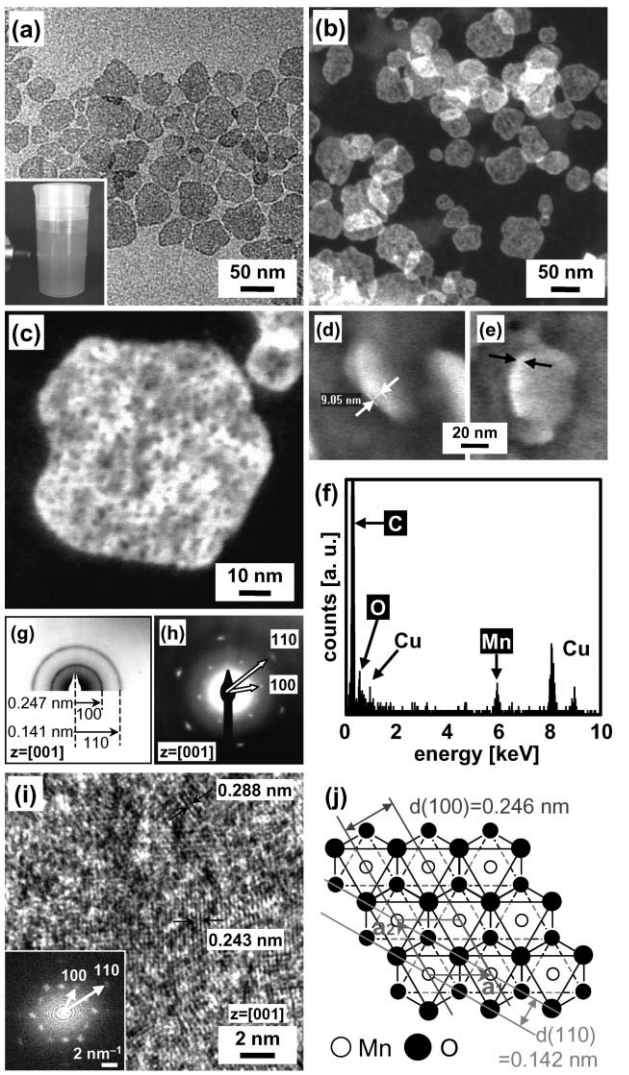

Fig. 1 Overview of manganese oxide nanoflakes with a mosaic structure. (a) FETEM images of the nanoflakes and their dispersed liquid exhibiting Tyndall light scattering (inset); (b and c) HAADF-STEM and magnified images of the flakes showing a mosaic structure; (d and e) FESEM images of flakes dropped on a glass slide; (f) EDX spectrum collected from the nanoflakes; (g and h) SAED patterns taken from the area including several flakes and a nanoflake; (i) HRTEM and its FFT images (inset); (j) Schematic model of the birnessite monolayer consisting of MnO_6 octahedrons.

caused by the grid with the collodion membrane in FETEM analysis (Fig. 1f). On the other hand, random aggregates with a sheet-like morphology and cubic Mn_3O_4 were obtained in the absence of PAA, and nanoflakes with a mosaic structure were not observed (Fig. S1 in ESI†).

According to the following analysis, the structure of the flakes was assigned to be a hexagonal birnessite-type manganese oxide containing sodium and/or water. Birnessite-type manganese oxide consists of two-dimensional monolayers of edge-shared MnO_6 octahedrons, and the interlayer space intercalates alkali metal ions and/or water molecules.[23,27–29] It has been reported that divalent manganese ions are easily oxidized in a basic solution.[30] Although the structure of birnessite has been well-investigated in previous reports,[23,27] morphological control on a nanoscopic scale was not fully demonstrated.

When the electron beam was irradiated perpendicularly to the flake, Debye–Scherrer rings were observed in the selected area, including several flakes (Fig. 1b,g). The hexagonal spots acquired from a nanoflake strongly indicated that the oriented architecture was formed with nanocrystals (Fig. 1c,h). The lattice spacing of 0.247 nm and 0.141 nm can be assigned to the (100) and (110) planes of birnessite, respectively (Fig. 1g,h). We recognized the same lattice spacing, such as 0.243 nm and 0.144 nm, in the HRTEM image (Fig. 1i). The spotted FFT image also supported the oriented architecture of nanocrystals in the flake (Fig. 1c,i). The structure of the nanoflakes was consistent with that of birnessite monolayers consisting of edge-shared MnO_6 octahedrons (Fig. 1j). The subsequent EELS analysis suggested the presence of sodium in the nanoflakes (Fig. 2a). The structure would be similar to that of Na-birnessite: the sodium ions are intercalated in the interlayer spaces.[27,29]

No powdered and dried samples were collected for further analysis because the nanoflakes were not centrifuged from the dispersion liquid. Thus, the nanoflakes were dropped on a glass or a silicon substrate by simply dipping (Fig. 2b). The FT-IR spectrum was collected from the samples on a silicon substrate by the reflectance mode (Fig. 2c). Commerical PAA powders of acid and sodium salts respectively showed the characteristic absorption bands resulting from dissociation

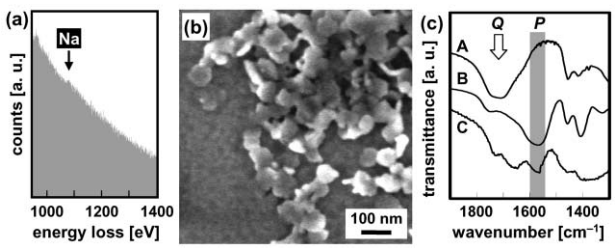

Fig. 2 Inclusion of sodium ions and PAA in manganese oxide nanoflakes. (a) EELS profile displaying the characteristic edge energy of Na–K at around 1100 eV; (b) FESEM image of the nanoflakes dropped on a glass slide; (c) FT-IR spectrum of PAA acid salt (A), PAA sodium salt (B), and the manganese oxide–PAA composite (C). The absorption bands P (1550–1600 cm^{-1}) and Q (1750–1800 cm^{-1}) indicate the carboxylate and carboxylic groups in PAA molecules, respectively.

behavior (Fig. 2c). The absorption band around 1570 cm^{-1} suggested that the carboxy groups of the PAA molecules were mainly dissociated to carboxylate anions, even though the presence of carboxylic groups was also recognized in the spectra (Fig. 2c). Therefore, it is inferred that PAA molecules coordinate to manganese species and/or interact with sodium, resulting in the control of crystal structure and morphology. According to these facts, nanoflakes with a mosaic interior are birnessite-type manganese oxide containing sodium and have the oriented architecture of nanocrystals with the incorporation of PAA. However, we could not carry out a structural analysis, particularly, in terms of the structure in the thickness direction and the sodium content. Further analysis and the manipulation of the nanoflakes are future challenges to their application in various devices.

3.2. Synthesis and characterization of cobalt hydroxide nanoflakes

Similar nanoflakes were synthesized in a different system using $Co(OH)_2$ and PEI (Fig. 3). The precursor solution containing Co^{2+} and PEI took on a light-brown color because of the complexation and immediately changed to dark blue upon addition of NaOH. The resultant solution gradually became a clear reddish-purple, exhibiting Tyndall light scattering (inset of Fig. 3a). Hexagonal nanoflakes less than 100 nm in size formed in the dispersion liquid (Fig. 3a). Since rough facets were observed in the magnified FETEM images, the nanoflakes were generated from tiny crystals less than 5 nm in size (Fig. 3b,c). The thickness of a nanoflake was estimated to be approximately 10 nm by FESEM images (Fig. 3d,e). In contrast, faceted hexagonal plates with various sizes were observed in the absence of PEI (Fig. S2 in ESI†). Although platy morphologies of $Co(OH)_2$ were fabricated in earlier works,[31–34] designing the interior form in nanoscale is also an important issue for application.

The EDX spectrum indicated the presence of carbon, oxygen, and cobalt in the nanoflakes (Fig. 3f). The carbon peak was enhanced in the spectrum, as was the case with manganese oxide. Thus, the structure was characterized as a $Co(OH)_2$–PEI composite containing sodium ions and water molecules between the brucite-type monolayers.[35,36] While Debye–Scherrer rings were observed in the area including several flakes (Fig. 3a,g), a nanoflake exhibited a hexagonal spotted pattern (Fig. 3c,h). In consequence, we concluded that the nanocrystals made up the oriented architecture in the flake with a mosaic structure. Through the analysis of several SAED patterns, the spacing of the (100) and (110) planes ranges from 0.251 to 0.264 nm and from 0.136 to 0.154 nm, respectively. HRTEM and its FFT images also showed similar lattice spacing, such as 0.280 nm and 0.316 nm (Fig. 3i,j). After centrifugation, the XRD pattern of the wet slurry was assignable to that of β-$Co(OH)_2$ (Fig. 3k). The peak resulting from the basal spacing of the (001) plane, 0.467 nm, became slightly broader and shifted from that in β-$Co(OH)_2$, 0.464 nm (Fig. S3 in ESI†). The shifts of the lattice spacing, as observed in the SAED and XRD patterns, can be ascribed to the intercalation of sodium ions and/or the incorporation of PEI. The FT-IR spectrum also showed the characteristic absorption

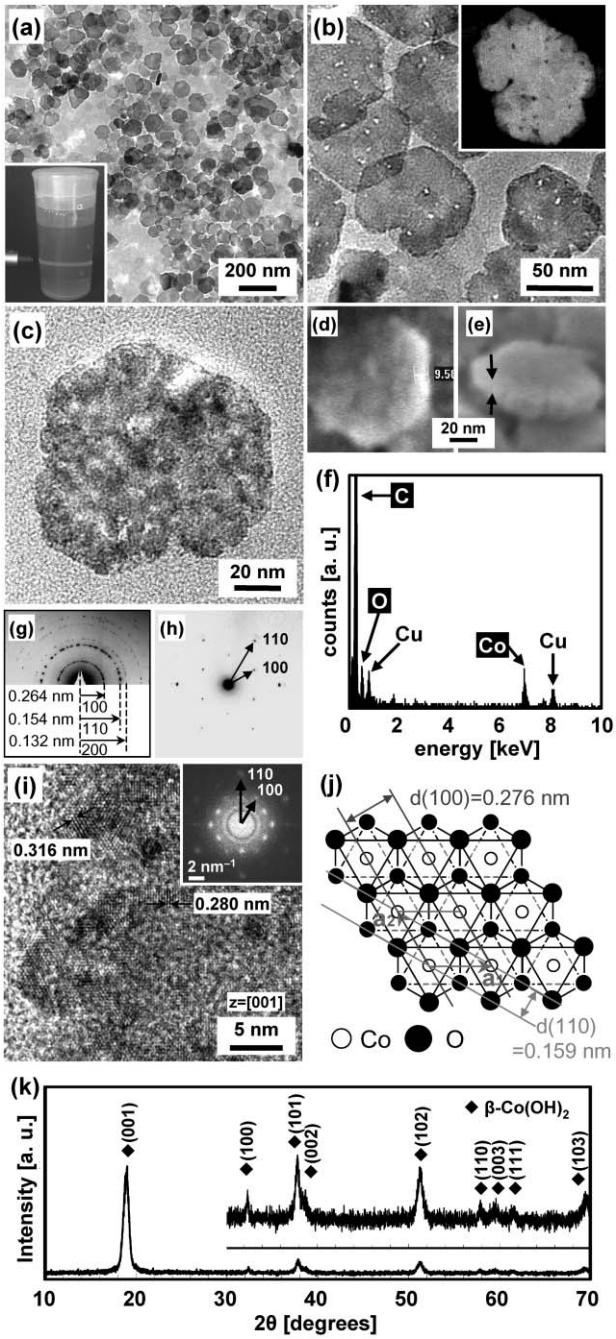

Fig. 3 Overview of cobalt hydroxide nanoflakes with a mosaic structure. (a) FETEM images of the nanoflakes and their dispersed liquid (inset); (b and c) FETEM and HAADF-STEM (inset) images of the mosaic structure; (d and e) FESEM images of flakes dropped on a glass slide; (f) EDX spectrum collected from the nanoflakes; (g and h) SAED patterns taken from the area including several flakes and a nanoflake; (i) HRTEM and its FFT image (inset); (j) Schematic model of the brucite monolayer consisting of CoO_6 octahedrons; (k) XRD pattern of the wet slurry after centrifugation of the dispersion liquid.

bands of the brucite structure (Fig. 4a). These results supported the idea that the brucite-type structure with an octahedral coordination of cobalt formed the nanoflakes (Fig. 3j). The nanocrystals made up the oriented architectures of brucite-type $Co(OH)_2$ exhibiting (001) faces.

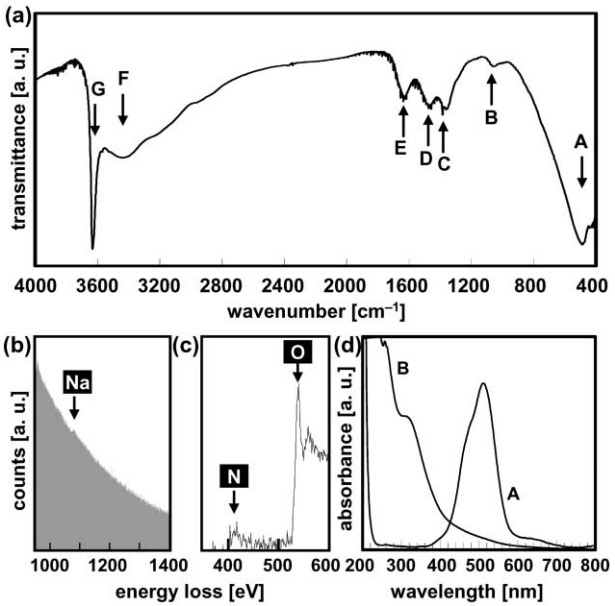

Fig. 4 Inclusion of sodium ions and PEI in cobalt hydroxide nanoflakes. (a) FT-IR spectrum of the dried nanoflakes. The absorption bands A and G are characteristic of a brucite-like sheet structure consisting of CoO_6 octahedrons: (A) Co–O stretching and Co–OH bending vibrations, (G) O–H stretching mode in the brucite structure. The inclusion of carbonate ions was recognized in the absorption bands B–D. The bands E and F were attributed to the water molecules in the interlayer space and/or to the adsorbed species. The peak assignment was referred to by earlier works.[8,31,33] (b and c) EELS and the background-subtracted profiles corresponding to the characteristic edge energies of Na–K and N–K, respectively; (d) UV-Vis spectra of the solution containing Co^{2+} (A) and Co^{2+}/PEI (B). The absorption band at around 350 nm resulted from the coordination of –NH– groups in PEI to Co^{2+} ions.

The presence of sodium was recognized in the EELS profiles (Fig. 4b). Comparing β-$Co(OH)_2$ to $Na_{0.74}CoO_2$ in the XRD patterns, the inclusion of sodium in the interlayer spaces results in an increase and a decrease in the spacing of the (00*l*) and (*h*00) planes, respectively (JCPDS #30-443 and ICDD #87-274). Therefore, the nanoflakes were deduced to be brucite-type β-$Co(OH)_2$ with the intercalation of small amounts of sodium ions in the interlayer space.

In the FT-IR spectrum, carbonate ions and water molecules were also contained in the resultant materials, as commonly observed in the synthesis of cobalt hydroxide (Fig. 4a).[8,31,33] However, the absorption bands resulting from PEI molecules could not be detected in the FT-IR spectrum because the broadened bands of the hydroxy groups and interlayer water molecules were overlapped (Fig. 4a). The presence of PEI was recognized by using other methods. The nitrogen in PEI was also detected in EELS analysis (Fig. 4b). A UV-Vis spectrum suggested complexation between –NH– groups in PEI and cobalt ions in the precursor solution (Fig. 4c): the coordination was characterized to the absorption band around 350 nm.[32] In the elemental analysis, the presence of *ca.* 0.9% nitrogen suggests that approximately 3 wt% of PEI molecules were accompanied by the nanoflakes. Therefore, the flakes with a brucite structure were composed

of oriented architectures of nanograins with the incorporation of PEI molecules.

4. Discussion

4.1. Roles of organic polymers

We successfully synthesized hierarchically structured nanomaterials through a biomimetic pathway under ambient conditions. As discussed in the previous sections, the organic polymers coordinated to the metal species in the precursor solution and were then incorporated in the mosaic nanoflakes. We recently reported the formation of zinc oxide nanowires with a mosaic structure in an aqueous solution: sulfate groups in organic molecules mediated the morphogenesis through interaction with the zinc species.[37] In the present study, we selected the polymers in anticipation of specific interaction between the metal ions and the functional groups. The interaction of the functional groups with the metal species can be ascribed to the strength of the Lewis acid and base in the combination. The organic molecules coordinate to metal ions in the precursor solutions and then interact with a specific crystal face. The interaction in the precursor solution inhibits rapid precipitation and then gradually supplies the metal species stabilized by the organic polymers. When the reaction started without organic polymers, a precipitate was immediately produced (Figs S1 and S2 in ESI†). Since the metal oxide nanostructures concurrently form from the precursor species, the resultant morphologies were controlled with organic molecules. These two interaction styles contribute to the controlling of the reaction rate and then directly to the design of the morphology and oriented structure. According to these model cases, tailoring an appropriate interaction is required for the generation of nanoscopic structures through a biomimetic route.

4.2. Proposed formation mechanisms

The formation of oriented architecture has been a focus of recent studies in terms of the nonclassical crystallization process.[18,19] The mosaic and oriented structures of nanocrystals may be ascribed to the oriented attachment or mesocrystal, implying that self-assembly of primary nanoparticles results in a highly organized structure with a specific crystal orientation.[18,19] The presence of organic molecules assists the aligmnent of building blocks with the generation of an electric dipole moment. However, isolated nanoparticles as the building blocks were not observed in the two nanoflakes in this study. The other formation process would lie in the morphogenesis of nanoflakes with a mosaic interior.

We previously demonstrated nanoscopic structures of biominerals and their biomimetic materials and have proposed another mechanism for the generation of oriented architectures, namely bridged nanocrystals.[21,22] According to the model, the morphogenesis proceeds through crystal growth with the association of organic molecules.[21a] As described in the previous section, the precursor metal species are gradually supplied because of the strong interaction with the organic polymers. A certain size of nanocrystal forms in the initial stage with the interaction of the organic polymer. Thus, the growth is temporarily inhibited by a specific interaction of the organic polymer. The growth restarts from the defect sites of the adsorption because the adsorbed organic polymers can not perfectly inhibit the growth in the precursor solution. The adjacent nanocrystals are induced with the formation of bridges, as was the case with our previous studies. Then, the growth of the nanocrystals is inhibited by the polymer again. In this way, stepwise growth, including inhibition and restarting, leads to the formation of oriented architecture with incorporation of the organic polymer *via* the bridges between each nanocrystal.[21a] The emergence of mosaic and oriented architecture can be attributed to this model. However, we could not conclude the mechanisms of crystal orientation because the early stage of crystallization was not observed in the rapid deposition of manganese oxide and cobalt hydroxide systems. Another question is why the size of each nanocrystal was confined to several nanometers. Further investigation is required for the understanding of oriented architectures, especially in the formation process.

5. Conclusions

We successfully synthesized manganese oxide and cobalt hydroxide nanoflakes in an aqueous solution containing organic polymers through a biomimetic process. These flakes, with mosaic interiors, were generated from the oriented architecture of nanocrystals with the incorporation of polymers. The hierarchically organized structures consisting of nanocrystals were formed through a bottom up approach, as was the case with biomineralization. The tailored association of organic polymers, including coordination and interaction to the metal species, led to the morphological design of manganese oxide and cobalt hydroxide nanoflakes in this study. The morphogenesis at a nanoscopic scale can be ascribed to stepwise crystal growth including inhibition and restarting, as previously proposed in our report. Moreover, this approach, based on an exquisite association of organic molecules, can be widely applied to the synthesis of metal oxide nanomaterials through a biomimetic route.

Acknowledgements

This work was supported by the 21st Century COE program "KEIO Life Conjugated Chemistry" from the Ministry of Education, Culture, Sports, Science, and Technology, Japan, and the Murata Science Foundation. One of the authors (Y. O.) thanks the JSPS for a research fellowship for young scientists.

References

1 T. Sasaki, S. Nakano, S. Yamauchi and M. Watanabe, *Chem. Mater.*, 1997, **9**, 602.
2 N. Sakai, Y. Ebina, K. Takada and T. Sasaki, *J. Am. Chem. Soc.*, 2004, **126**, 5851.
3 R. Ma, Y. Bando and T. Sasaki, *J. Phys. Chem. B*, 2004, **108**, 2115.
4 A. Shimojima and K. Kuroda, *Chem. Rec.*, 2006, **6**, 53.
5 D. Mochizuki, A. Shimojima, T. Imagawa and K. Kuroda, *J. Am. Chem. Soc.*, 2005, **127**, 7183.
6 W. Sugimoto, H. Iwata, Y. Yasunaga, Y. Murakami and Y. Takasu, *Angew. Chem., Int. Ed.*, 2003, **42**, 4092.

7 E. Hosono, S. Fujihara, I. Honma and H. Zhou, *Adv. Mater.*, 2005, **17**, 2091.
8 E. Hosono, S. Fujihara, I. Honma and H. Zhou, *J. Mater. Chem.*, 2005, **15**, 1938.
9 S. Fujihara, E. Hosono and T. Kimura, *J. Sol–Gel Sci. Technol.*, 2004, **31**, 165.
10 M. Wei, H. Sugihara, I. Honma, M. Ichihara and H. Zhou, *Adv. Mater.*, 2005, **17**, 2964.
11 S. H. Yu and M. Yoshimura, *Adv. Mater.*, 2002, **14**, 296.
12 M. Niederberger, F. Krumeich, K. Hegetschweiler and R. Nesper, *Chem. Mater.*, 2002, **14**, 78.
13 L. Zhang, D. Chen and X. Jiao, *J. Phys. Chem. B*, 2006, **110**, 2668.
14 U. K. Gautam, M. Ghosh and C. N. R. Rao, *Langmuir*, 2004, **20**, 10775.
15 C. C. Li, W. P. Cai, B. Q. Cao, F. Q. Sun, Y. Li, C. X. Kan and L. D. Zhang, *Adv. Funct. Mater.*, 2006, **16**, 83.
16 C. Yan and D. Xue, *J. Phys. Chem. B*, 2005, **109**, 12358.
17 M. Antonietti and G. A. Ozin, *Chem.–Eur. J.*, 2004, **10**, 28.
18 H. Cölfen and S. Mann, *Angew. Chem., Int. Ed.*, 2003, **42**, 2350.
19 (*a*) M. Niederberger and H. Cölfen, *Phys. Chem. Chem. Phys.*, 2006, **8**, 3271; (*b*) H. Cölfen and M. Antonietti, *Angew. Chem., Int. Ed.*, 2005, **44**, 5576 and references therein.
20 (*a*) S. Mann, *Biomineralization*, Oxford University Press, Oxford, 2001; (*b*) S. H. Yu and H. Cölfen, *J. Mater. Chem.*, 2004, **14**, 2124 and references therein.
21 (*a*) Y. Oaki, A. Kotachi, T. Miura and H. Imai, *Adv. Funct. Mater.*, 2006, **16**, 1633; (*b*) Y. Oaki and H. Imai, *Small*, 2006, **2**, 66; (*c*) Y. Oaki and H. Imai, *Angew. Chem., Int. Ed.*, 2005, **44**, 6571.
22 (*a*) Y. Oaki and H. Imai, *Adv. Funct. Mater.*, 2005, **15**, 1407; (*b*) Y. Oaki and H. Imai, *Chem. Commun.*, 2005, 6011; (*c*) T. Miura, A. Kotachi, Y. Oaki and H. Imai, *Cryst. Growth Des.*, 2006, **6**, 612.
23 Q. Feng, H. Kanoh and K. Ooi, *J. Mater. Chem.*, 1999, **9**, 319 and references therein.
24 X. F. Shen, Y. S. Ding, J. Liu, J. Cai, K. Laubernds, R. P. Zerger, A. Vasiliev, M. Aidow and S. L. Suib, *Adv. Mater.*, 2005, **17**, 805.
25 C. Julien and M. Massort, *Phys. Chem. Chem. Phys.*, 2002, **4**, 4226.
26 M. Wei, Y. Konishi, H. S. Zhou, H. Sugihara and H. Arakawa, *Nanotechnology*, 2005, **16**, 245.
27 (*a*) X. Yang, Y. Makita, Z. Liu, K. Sakane and K. Ooi, *Chem. Mater.*, 2004, **16**, 5581; (*b*) X. Yang, W. Tang, Q. Feng and K. Ooi, *Cryst. Growth Des.*, 2003, **3**, 409; (*c*) Q. Feng, L. Liu and K. Yanagisawa, *J. Mater. Sci. Lett.*, 2000, **19**, 1567; (*d*) Q. Feng, E. H. Sun, K. Yanagisawa and N. Yamasaki, *J. Ceram. Soc. Jpn.*, 1997, **105**, 564.
28 (*a*) L. Wang, K. Takada, A. Kajiyama, M. Onoda, Y. Michiue, L. Zhang, M. Watanabe and T. Sasaki, *Chem. Mater.*, 2003, **15**, 4508; (*b*) Y. Omomo, T. Sasaki, L. Wang and M. Watanabe, *J. Am. Chem. Soc.*, 2003, **125**, 3568.
29 J. P. Parant, R. Olazcuaga, M. Devalette, C. Fouassier and P. Hagenmuller, *J. Solid State Chem.*, 1971, **3**, 1.
30 (*a*) A. R. Nichols and J. H. Walton, *J. Am. Chem. Soc.*, 1942, **64**, 1866; (*b*) A. Vázquez-Olmos, R. Redón, G. Rodriguez-Gattorno, M. E. Mata-Zamora, F. Morales-Leal, A. L. Fernández-Osrio and J. M. Saniger, *J. Colloid Interface Sci.*, 2005, **291**, 175.
31 Z. Liu, R. Ma, M. Osada, K. Takada and T. Sasaki, *J. Am. Chem. Soc.*, 2005, **127**, 13869.
32 J. T. Sampanthar and H. C. Zeng, *J. Am. Chem. Soc.*, 2002, **124**, 6668.
33 Y. Zhu, H. Li, Y. Koltypin and A. Gedanken, *J. Mater. Chem.*, 2002, **12**, 729.
34 Y. Hou, H. Kondoh, M. Shimojo, T. Kogure and T. Ohta, *J. Phys. Chem. B*, 2005, **109**, 19094.
35 (*a*) R. L. Penn, A. T. Stone and D. R. Veblen, *J. Phys. Chem. B*, 2001, **105**, 4690; (*b*) C. Fouassier, G. Matejka, J. M. Reau and P. Hagenmuller, *J. Solid State Chem.*, 1973, **6**, 532.
36 K. Takada, M. Osada, F. Izumi, H. Sakurai, E. Takayama-Muromachi and T. Sasaki, *Chem. Mater.*, 2005, **17**, 2034.
37 J. Yahiro, Y. Oaki and H. Imai, *Small*, 2006, **2**, 1183–1187.